iScience

CellPress
OPEN ACCESS

Article

Biomimetic proteolipid vesicles for reverting GPI deficiency in paroxysmal nocturnal hemoglobinuria

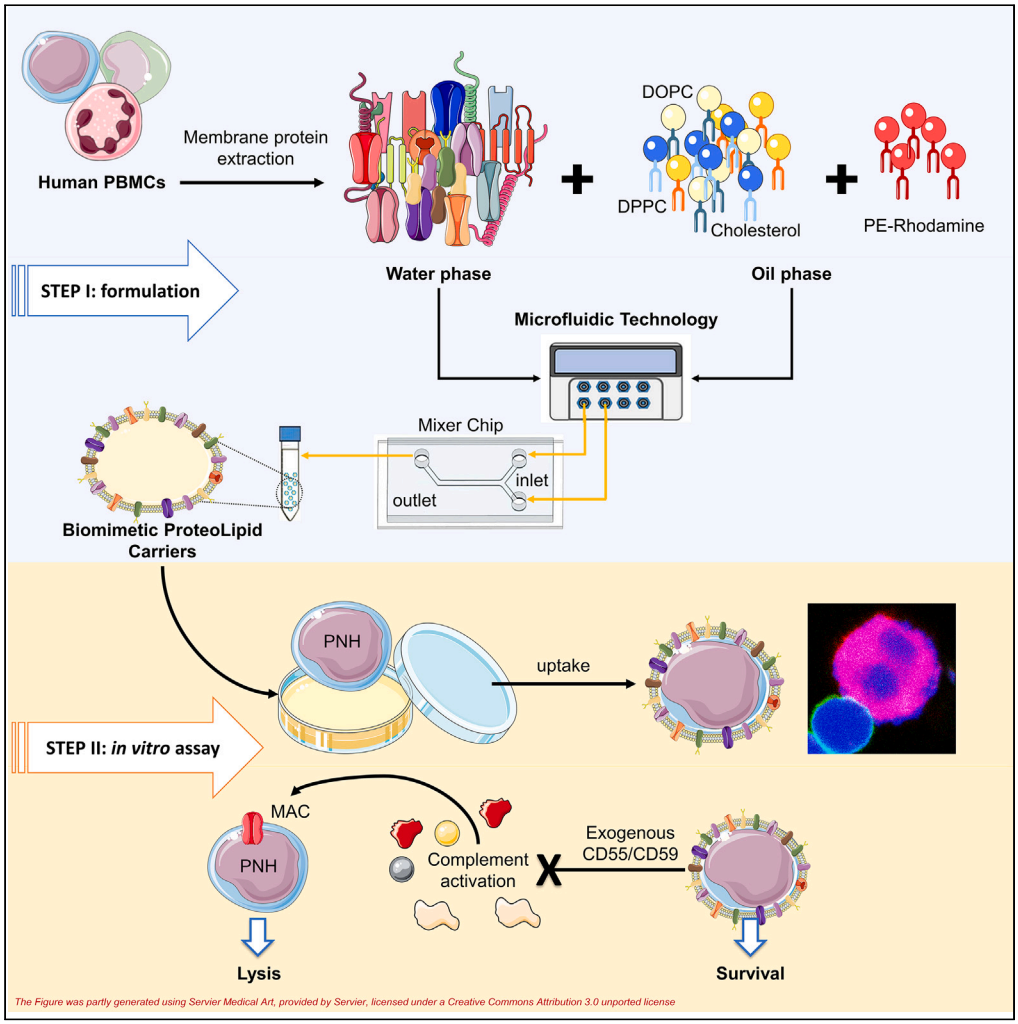

Valentina Giudice, Pasqualina Scala, Erwin P. Lamparelli, ..., Francesca Picone, Giovanna Della Porta, Carmine Selleri

gdellaporta@unisa.it

Highlights

Microfluidic technology allows formulation of biomimetic proteolipid vesicles

Biomimetic vesicles can be functionalized with human GPI-anchored proteins

Biomimetic functionalized vesicles can deliver GPI-linked proteins to cells

Treated PNH cells have increased resistance to complement-mediated lysis

Giudice et al., iScience 27, 109021
March 15, 2024
https://doi.org/10.1016/j.isci.2024.109021

iScience

CellPress
OPEN ACCESS

Article

Biomimetic proteolipid vesicles for reverting GPI deficiency in paroxysmal nocturnal hemoglobinuria

Valentina Giudice,[1,2,4] Pasqualina Scala,[1,4] Erwin P. Lamparelli,[1] Marisa Gorrese,[1] Bianca Serio,[2] Angela Bertolini,[1] Francesca Picone,[1] Giovanna Della Porta,[1,3,5,*] and Carmine Selleri[1,2]

SUMMARY

Nano-vesicular carriers are promising tissue-specific drug delivery platforms. Here, biomimetic proteolipid vesicles (BPLVs) were used for delivery of glycosylphosphatidylinositol (GPI)-anchored proteins to GPI deficient paroxysmal nocturnal hemoglobinuria (PNH) cells. BPLVs were assembled as single unilamellar monodispersed (polydispersity index, 0.1) negatively charged (ζ-potential, −28.6 ± 5.6 mV) system using microfluidic technique equipped with Y-shaped chip. GPI-anchored and not-GPI proteins on BPLV surface were detected by flow cytometry. Peripheral blood mononuclear cells (PBMCs) from healthy and PNH subjects were treated with BPLVs (final concentration, 0.5 mg/mL), and cells displayed an excellent protein uptake, documented by flow cytometry immunophenotyping and confocal microscopy. BPLV-treated cells stressed with complement components showed an increased resistance to complement-mediated lysis, both healthy and PNH PBMCs. In conclusion, BPLVs could be effective nanocarriers for protein transfer to targeted cells to revert protein deficiency, like in PNH disease. However, further *in vivo* studies are required to validate our preclinical *in vitro* results.

INTRODUCTION

Bone marrow failure (BMF) syndromes, a heterogeneous group of benign hematological diseases, are characterized by bone marrow (BM) aplasia and peripheral blood cytopenia(s) and can be caused by inherited germline mutations in the hematopoietic stem and progenitor cell (HSPC) compartment (constitutional syndromes) or by extrinsic direct and indirect damages on HSPCs (acquired conditions).[1–4] Within acquired BMF syndromes, paroxysmal nocturnal hemoglobinuria (PNH) is caused by somatic mutations in the X-linked phosphatidyl-inositol glycan class A (*PIGA*) gene affecting glycosylphosphatidylinositol (GPI) anchor biosynthesis and leading to various degree of GPI deficiency. Consequently, proteins requiring GPI-anchor to correctly localize on cell surface fail to be expose on surface membrane, and cells carrying *PIGA* mutations completely lack the entire subset of GPI-anchored proteins, including complement regulatory proteins CD55 and CD59.[5] Therefore, GPI deficient cells are more susceptible to complement-mediated cell lysis, which is the main pathogenetic event of PNH-related symptoms (anemia, hemoglobinuria, and thrombosis). However, to date, the only pharmacologically active targeted therapy for treatment of PNH patients is complement inhibition, that reduces the rate of complement activation ultimately decreasing GPI-deficient cell lysis.[4,5]

Lipid nanoparticles are the new frontier of drug delivery because they successfully overcome commonly drug delivery issues, such as poor bioavailability, short half-life, drug instability, possible side effects, and the lack of targeted delivery. Lipid nanoparticles can be fabricated using different technologies, such as thin-film hydration, supercritical fluid processes, or microfluidic approaches.[6–9] In microfluidics protocols, ethanol and water phases are mixed within micro-channels, and unilamellar monodispersed nanovesicles are obtained if process parameters, such as flow rates and flow rate ratios, are well-optimized.[10,11] Microfluidics approaches also allow scale-up feasibility, enhanced encapsulation efficiency, and excellent batch-to-batch reproducibility if compared to other technologies, as well as great stability in suspension over time.[12] Lipid nano-carriers often showed low systemic toxicity and can be used to formulate injectable system, as documented by several commercial formulations with several encapsulated drugs, such as anticancer molecules, antibiotics, antifungal drugs, or anesthetics, and nucleic acids or mRNA vaccine purposes.[13,14]

Lipid nano-vesicles contents are generally delivered by endocytosis, while bigger lipid vesicles (150–300 nm) can fuse with cell membrane and release their load within cytoplasm.[15] However, carriers are recognized as non-self-particles by immune cells that quickly remove them from the bloodstream, preventing their access to target tissues.[16] Targeting efficiency can be increased by functionalizing nano-vesicles surface with specific molecules and ligands, which can guide and bind ligands on targeted tissues, like leukocyte-derived adhesion molecules for selective targeting of inflamed endothelium.[17,18] Among functionalized liposomes, biomimetic leukocyte-like nanocarriers appear as a

[1]Department of Medicine, Surgery, and Dentistry, University of Salerno, Baronissi, Italy
[2]Hematology and Transplant Center, University Hospital "San Giovanni di Dio e Ruggi d'Aragona", Salerno, Italy
[3]Interdepartment Centre BIONAM, University of Salerno, Fisciano, Italy
[4]These authors contributed equally
[5]Lead contact
*Correspondence: gdellaporta@unisa.it
https://doi.org/10.1016/j.isci.2024.109021

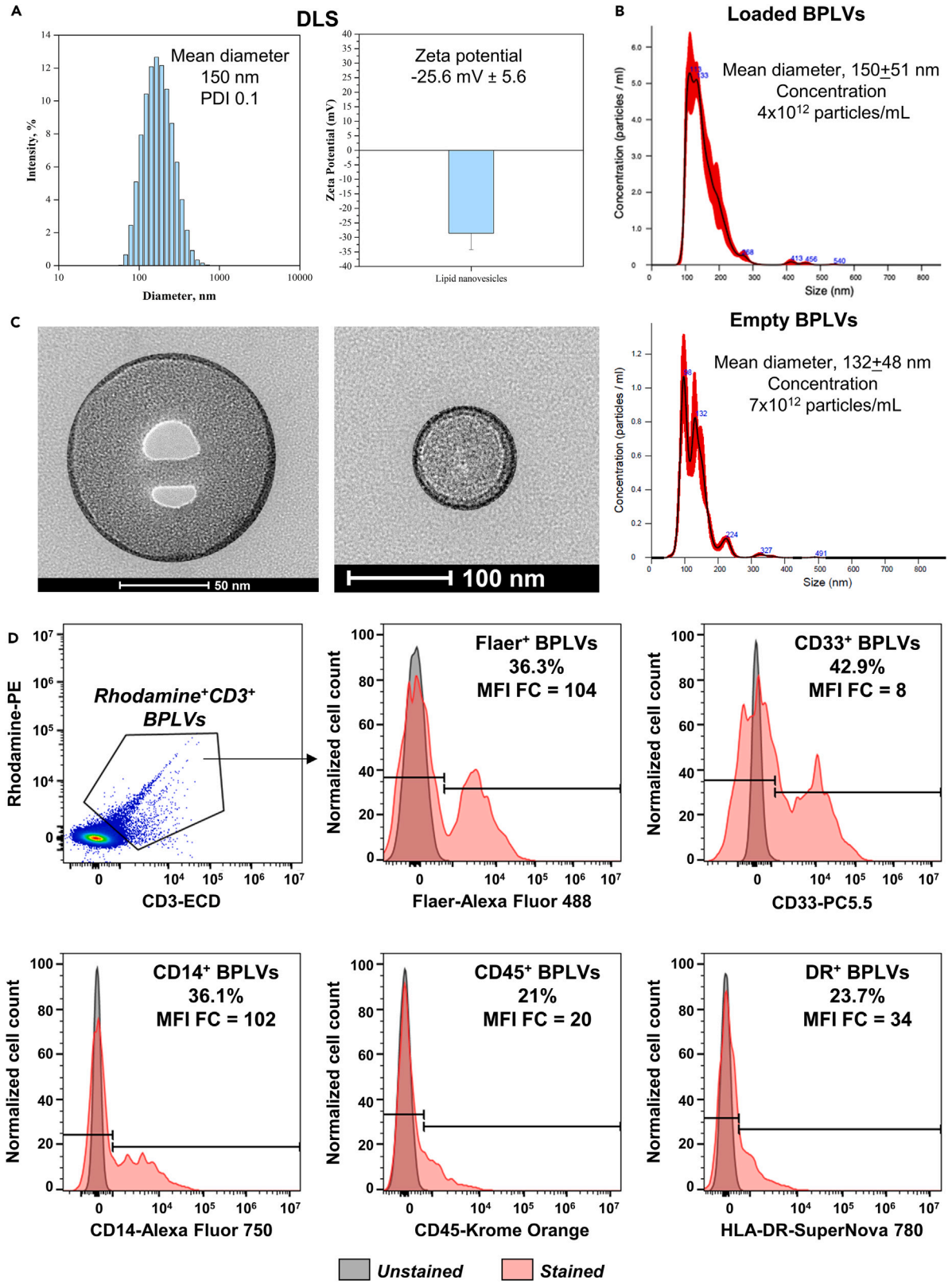
A
DLS
Mean diameter
150 nm
PDI 0.1
Intensity, %
Diameter, nm
Zeta potential
-25.6 mV ± 5.6
Zeta Potential (mV)
Lipid nanovesicles
B
Loaded BPLVs
Mean diameter, 150±51 nm
Concentration
4x10^12 particles/mL
Concentration (particles / ml)
Size (nm)
C
50 nm
100 nm
Empty BPLVs
Mean diameter, 132±48 nm
Concentration
7x10^12 particles/mL
Concentration (particles / ml)
Size (nm)
D
Rhodamine⁺CD3⁺
BPLVs
Rhodamine-PE
CD3-ECD
Flaer⁺ BPLVs
36.3%
MFI FC = 104
Normalized cell count
Flaer-Alexa Fluor 488
CD33⁺ BPLVs
42.9%
MFI FC = 8
Normalized cell count
CD33-PC5.5
CD14⁺ BPLVs
36.1%
MFI FC = 102
Normalized cell count
CD14-Alexa Fluor 750
CD45⁺ BPLVs
21%
MFI FC = 20
Normalized cell count
CD45-Krome Orange
DR⁺ BPLVs
23.7%
MFI FC = 34
Normalized cell count
HLA-DR-SuperNova 780
Unstained
Stained

Figure 1. Biomimetic proteolipid vesicle (BPLV) characterization

BPLVs were physically characterized by (A) dynamic light scattering (DLS) analysis showing a homogeneous population (polydispersity index, PDI) with a negative zeta potential, optimal for cell membrane interaction, and (B) by Nanosight confirming the homogenous distribution in size and obtaining particle concentration. Data are represented as mean ± standard deviation (SD).

(C) BPLV morphology was also studied by transmission electron microscopy and the lipidic layer was stained using a phosphotungstic acid solution (2% w/v) allowing the visualization of a unilamellar lipid layer in both empty (left panel) and loaded BPLVs (right panel).

(D) Surface protein expression on BPLVs was investigated by flow cytometry, and particles were first identified based on simultaneous presence of a rhodamine-tagged phospholipid and a human membrane protein (CD3). On these particles, percentage of Flaer$^+$, CD33$^+$, CD14$^+$, CD45$^+$, and HLA-DR$^+$ vesicles were calculated, as well as median fluorescence intensity (MFI) fold change was calculated by dividing MFI of stained sample/MFI of an unstained control.

novelty in the drug delivery field, and are obtained by integrating leukocyte-derived membrane proteins in synthetic lipid nanocarriers, resembling physiological leukocyte activities, such as cell adhesion, and regulation of inflammation. Indeed, these nano-vesicles have a great potential in reducing neutrophil infiltration and favoring inflammation resolution in *in vitro* and *in vivo* models.[18,19] For example, biomimetic leukocyte-like carriers were already reported to be produced by microfluidics approach.[20–22]

In this work, we formulated biomimetic proteolipid vesicles (BPLVs) for clinical purposes as a potential therapy for reverting GPI deficiency in PNH. We first optimized microfluidics condition for BPLV assembly and by mixing synthetic lipids and membrane proteins obtained by peripheral blood mononuclear cells (PBMCs) from healthy donors. Next, functionalized BPLVs were characterized in size, morphology, surface charge, and cytotoxicity, and subsequently tested *in vitro* for their therapeutic potential in PNH treatment on healthy and pathological human primary cells.

RESULTS

BPLV morphologic, physical, and phenotypical characterization

Microfluidic system was equipped with a Y-shaped staggered herringbone micromixer chip with an internal diameter of 600 μm (overall length, 10 mm), and flow rate was set at 4 mL/min, total lipid concentration in ethanol at 17.5 mg/mL (ethanol/water phase ratio, 1:2), and final lipid:protein ratio at 1:35. In details, organic phase was composed of 1,2-dipalmitoyl-*sn*-glycero-3-phosphocholine (DPPC), 1,2-dioleoyl-*sn*-glycero-3-phosphocholine (DOPC), and cholesterol. A labeled PE-rhodamine (1,2-dioleoyl-*sn*-glycero-3-phosphoethanolamine-N-lissamine rhodamine B sulfonyl) was added to lipid mixture at a concentration of 0.5% based on total lipid phase as a BPLV red tracer. The water phase was supplemented with total extract of membrane proteins obtained from healthy and PNH PBMCs. Reagents were then loaded in 15 mL tubes and connected to the microfluidics circuits, where preset pressures were directly applied, pushing solutions into the mixing chip with a total constant flow rate of 4 mL/min. Then, mixed solution was collected in a clean 15 mL tube end-connected to the chip. Flow rates lower or higher than 4 mL/min were also tested; however, vesicles with larger size distribution were obtained (data not shown). By using these conditions, obtained BPLVs had a mean diameter of 150 nm and a polydispersity index (PDI) of 0.1. Loaded BPLVs had a negative surface charge of −29mV and were obtained at concentration of $4.5x10^{12}$ particles/mL (Figures 1A and 1B). Empty vesicles showed same polydispersity of 0.1, with slightly lower mean size (132 nm) and higher concentration ($7.5x10^{12}$ particles/mL). High-magnification transmission electron microscope (TEM) microphotographs showed unilamellar BPLVs with a uniform surface, due to the presence of membrane proteins, which seemed also exposed on vesicle surface (Figure 1C). BPLV stability was also checked after storage at +4°C for three months, with no significant changes in composition and size of both empty and loaded vesicles; a slight increase of mean diameter of loaded vesicles was detected (168 nm), but with similar PDI value of 0.1.

Protein quantification on dialysis water by Bradford assay (indirect method) indicated undetectable proteins (<0.1 mg/mL), suggesting an extremely high encapsulation efficiency. Protein loading on BPLV surface was assessed by flow cytometry immunophenotyping for expression of GPI-anchored (Flaer and CD14) and not-GPI proteins (CD3, CD33, CD45, and HLA-DR) (Figure 1D). BPLVs were first identified as PE-rhodamine$^+$CD3$^+$ particles, and further characterization was conducted showing that BPLVs carried GPI-anchored proteins (Flaer$^+$ BPLVs, 36.3%; and CD14$^+$ BPLVs, 36.1%) and not-GPI proteins, including CD33 (42.9%), CD45 (21%), and HLA-DR (23.7%). Therefore, this system was chosen for assembly for subsequent studies.

BPLVs improve cell metabolism and viability

Several BPLV concentrations from 0.1 mg/mL to 2 mg/mL were tested to assess their cytotoxicity on healthy PBMCs (Figure 2). Lower concentrations and time (2 h, 4 h, 6 h, and 12 h) were also investigated showing lower cellular uptake (data not shown), thus higher concentrations and 24–72 h treatment were chosen for further investigations. Treatments with empty BPLVs at lower concentrations assured high cell viability more than 90% that decreased at 57% and at 39% after 1 mg/mL and 2 mg/mL treatments. Generally, cell viability was higher after treatments with loaded BPLVs. From 0.1 mg/mL to 1 mg/mL, viability values exceeded control, where the maximum peak was reached at the concentration of 0.5 mg/mL. Only in case of 2 mg/mL concentration, cell viability decreased at 52% (Figure 2A).

Since treatments with 0.5 mg/mL assured the highest cell viability on healthy PBMCs, this concentration was tested also on PNH PBMCs at 24 h, 48 h, and 72 h of culture. Empty BPLV treatments showed a cell viability of 58% after 24 h that progressively decreased at 47% and 18% at 48 h and 72 h, respectively. On the other end, when cells were treated with loaded BPLVs, cell viability was of 90% after 24 h, reached the maximum peak of 146% at 48 h and then 122% after 72 h of culture. Cytotoxicity on PNH PBMCs confirmed the good cell viability of loaded BPLVs at 0.5 mg/mL, especially after 48 h of culture, thus this concentration was chosen to further analysis (Figure 2B).

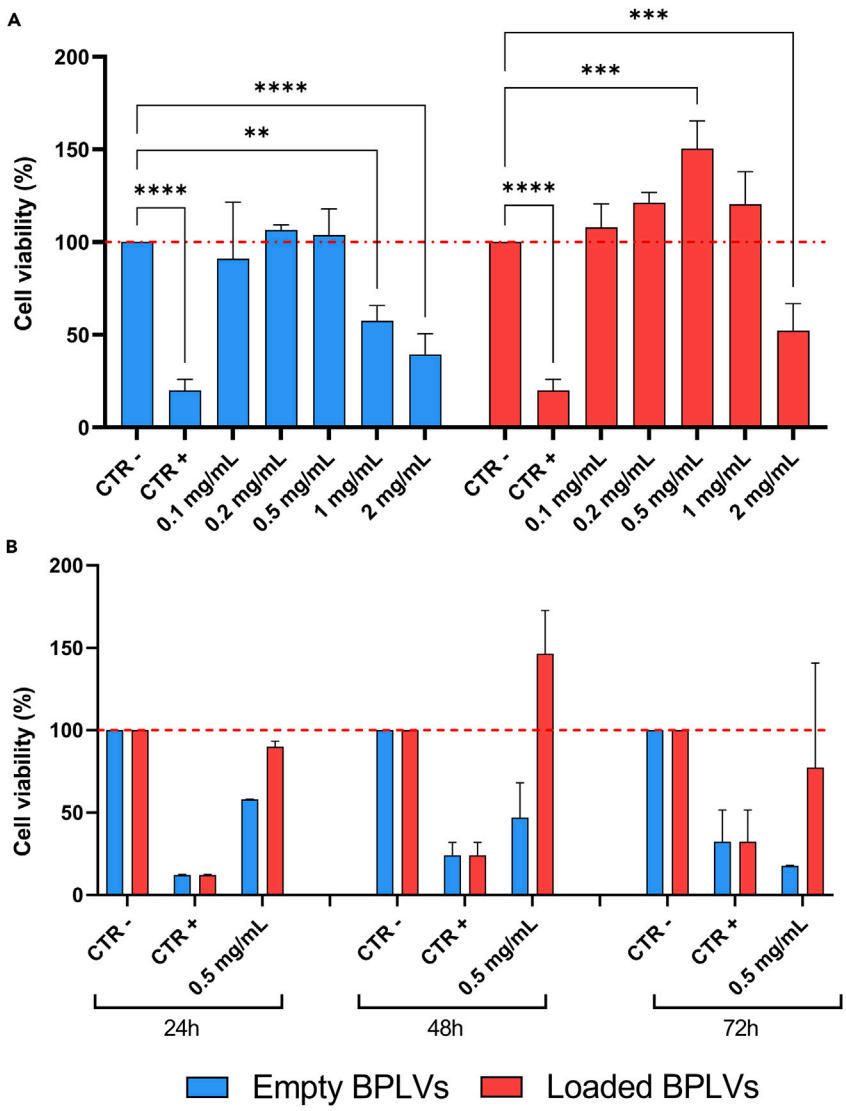

Figure 2. Cytotoxicity on healthy and paroxysmal nocturnal hemoglobinuria (PNH) peripheral blood mononuclear cells (PBMCs)

(A) Cells were treated with increasing concentrations of empty (without human membrane proteins) or loaded (with proteins) biomimetic proteolipid vesicles (BPLVs) for 24 h, and cell viability by 3-(4,5-dimethylthiazol-2-yl)-2,5-diphenyl- tetrazolium bromide (MTT) assay. A sample without BPLV treatment was used as negative control (CTR−), while a sample treated with dimethyl sulfoxide (DMSO) as positive control (CTR+).

(B) Cell viability was tested by MTT assay at 24 h, 48 h, and 72 h using a final concentration of 0.5 mg/mL of BPLVs. Data are represented as mean ± SD. **, $p < 0.01$; ***, $p < 0.001$; ****, $p < 0.0001$.

GPI-anchored proteins carried by BPLVs are efficiently incorporated in RBCs and PBMCs

First, cellular uptake of BPLVs was tested on different cell types, such as red blood cells (RBCs), PBMCs, and whole BM mononucleated cells (BMMCs), because RBCs are the most affected cells by complement-mediated lysis during PNH, while GPI$^-$ PBMCs also show functional modifications.[1] Therefore, whether to test the ability of BPLVs carried with GPI-anchored proteins to revert the PNH phenotype, we first explored cellular uptake by confocal microscopy and flow cytometry. Our BPLVs were tagged with PE-rhodamine for quick visualization and tracking, as BPLV$^+$ cells were visible in the PE signal (574 nm; red signals at confocal microscopy). RBCs displayed an excellent uptake just after 2 h of treatment, as PE-rhodamine signals were more intense than those of the lipophilic tracer, suggesting an active and avid uptake of vesicles by RBCs, compared to a passive conjugation to membrane lipid by N-hydroxysuccinimde (NHS) dye (Figure 3).

Next, BPLV uptake was tested on healthy and PNH PBMCs at T0, after 48 h and 72 h of culture without or with BPLVs (Figures 4 and 5), and PE-rhodamine-conjugated BPLVs and Flaer signals were investigated by confocal microscopy to visualize cellular uptake of vesicles (red signals) and co-localization with GPI-anchored proteins (green signals) carried by our BPLVs (co-localization indicated by a merged purple signal). An intense uptake was observed at 48 h and 72 h in both healthy and PNH PBMCs with

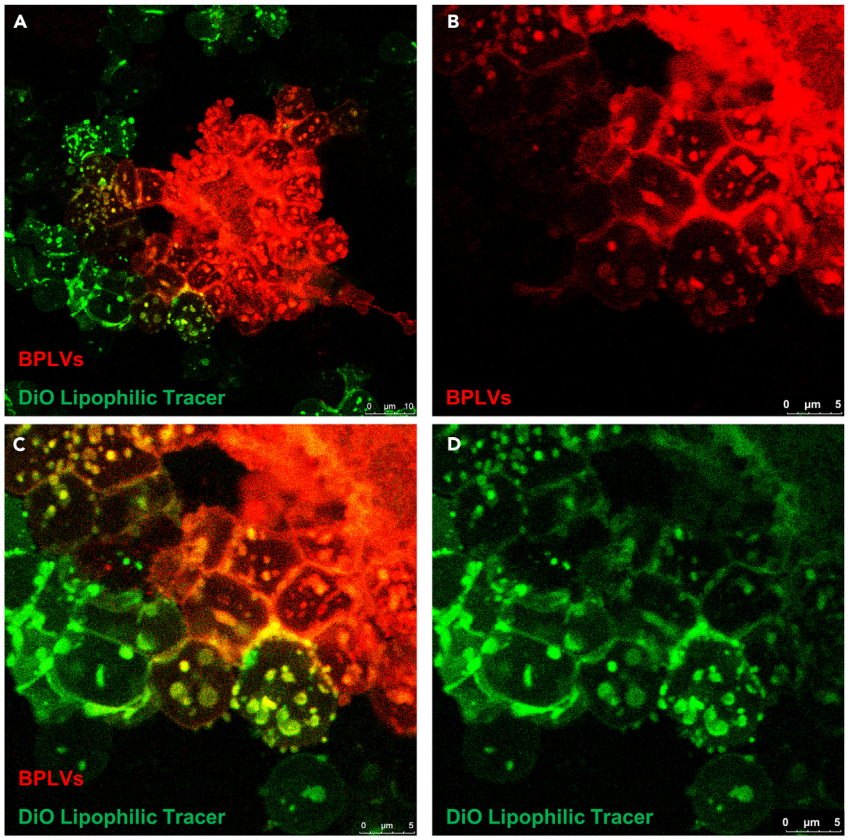

Figure 3. Biomimetic proteolipid vesicle (BPLV) uptake by red blood cells (RBCs)

Vesicle uptake was studied by confocal microscopy, as BPLVs were tagged with PE-rhodamine tracer (red signals), while RBC membranes with a lipophilic dye (DiO lipophilic tracer, green signals). RBCs that have uptake BPLVs showed an intense red or merged orange signals.

(A) RBC membranes are stained with DiO lipophilic tracer (green signal) and those RBCs that have uptaken PE-rhodamine BPLVs show a red or orange (merged) signal. Higher magnification (10X zoom) of RBCs for PE channel for BPLV uptake (B), FITC channel for membrane staining (D), and merged channels (C).

intracytoplasmic and membrane distribution of merged signals in more than 25% of cells/acquired field for healthy samples and ≥80% for PNH cells.

Cellular uptake of PE-rhodamine-conjugated BPLVs was also investigated by flow cytometry, especially for GPI-anchored protein delivery to targeted cells. For assessment of GPI-anchored protein expression, an FITC-conjugated Flaer was employed. Flaer, a mutated form of proaerolysin protein secreted by *Aeromonas hydrophila*, is activated by proteolysis, causing channel formation and lysis in GPI^+ cells while not in PNH cells, because this toxin binds to the GPI moiety of GPI-linked proteins.[23] FLAER is more sensitive than CD59 for detection of small clones (cut-off, 0.5%), except for RBC PNH clone identification; however, we also included another GPI-linked protein expression, CD14, combined with non-GPI-linked proteins, such as CD3 (for T lymphocytes), CD45 (pan-leukocyte marker), CD33 (for granulocytes), and HLA-DR. First, total $BPLV^+$ cells were identified to assess vesicle uptake by PBMCs, and PNH cells showed a surprisingly higher BPLV uptake compared to healthy cells (mean ± SD, 8.32 ± 6.04% vs. 2.1 ± 1.4%, respectively; $p = 0.0010$) (Figure 6A). Next, $Flaer^+BPLV^+$ cells were investigated, and frequencies were significantly higher in treated samples compared to untreated cells, as expected (mean ± SD in PNH, 0.03 ± 0.03% vs. 3.84 ± 2.9%, untreated vs. treated; $p < 0.0001$; and mean ± SD in healthy controls, 0.07 ± 0.1% vs. 2.76 ± 1.6%, untreated vs. treated; $p < 0.0001$) (Figure 6B). Subsequently, on PNH samples, we further investigated total $Flaer^+$ cells, based on the hypothesis that GPI-clone should decrease after treatment with BPLVs carrying GPI-linked proteins, as PNH cells should acquire the entire set of GPI-anchored proteins. Total $Flaer^+$ cells significantly increased after treatment (mean ± SD, 68.68 ± 10.8% vs. 72.46 ± 10.6%; $p = 0.0304$), especially after 48 h ($p = 0.0032$), while no differences were observed in healthy controls ($p = 0.1085$), as GPI^+ population was already ≥80% of total cells.

GPI-anchored protein expression was also studied by monitoring median fluorescence intensity (MFI) values of Flaer over culture time and by comparing the expression between PNH, healthy controls, and samples treated with empty vesicles (only synthetic lipids without membrane proteins) (Figure 6C). On $BPLV^+$ cells, Flaer expression significantly increased over culture time in PNH samples (mean MFI ± SD, 4528 ± 322 vs. 6510 ± 187 vs. 11053 ± 767, 24 h vs. 48 h vs. 72 h), after 48 h ($p = 0.0135$) and 72 h ($p = 0.0073$) of BPLV treatment. No significant variations were observed in healthy controls samples (mean MFI ± SD, 39218 ± 6986 vs. 26754 ± 5748 vs. 52654 ± 12449, 24 h vs. 48 h vs. 72 h; all $p > 0.05$), and in samples treated with empty vesicles (mean MFI ± SD, 17160 ± 15589 vs. 14760 ± 10881 vs. 14887 ± 8094, 24 h vs. 48 h vs.

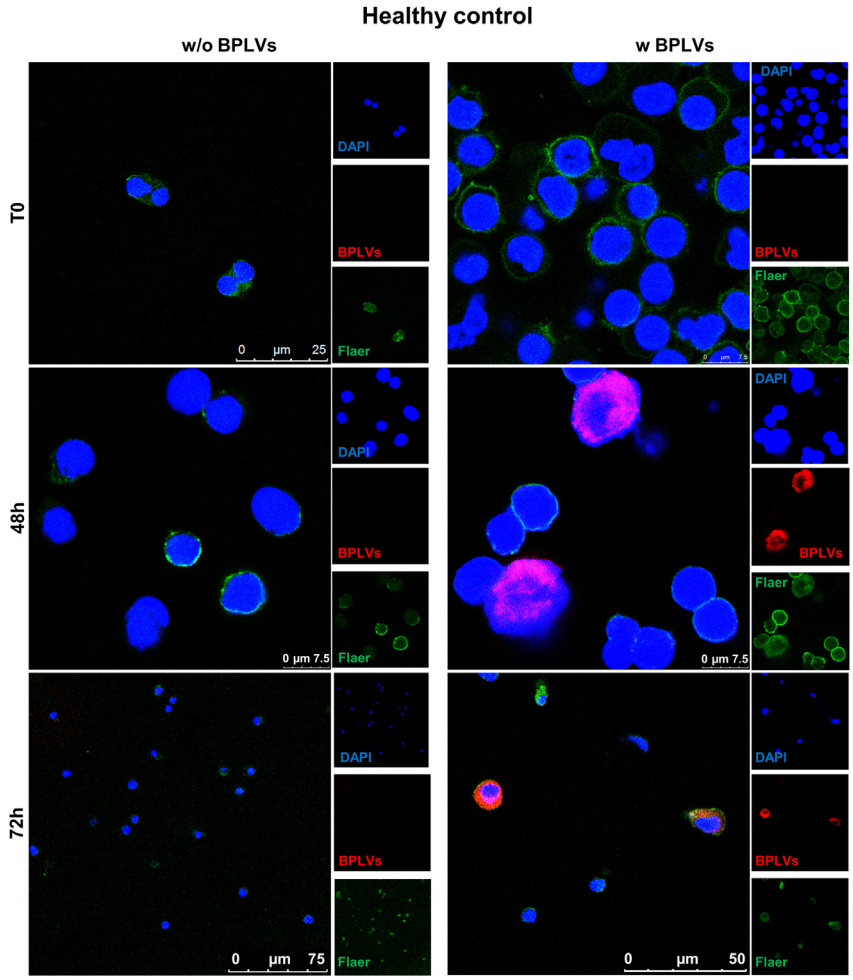

Figure 4. Biomimetic proteolipid vesicle (BPLV) uptake by healthy peripheral blood mononuclear cells (PBMCs)

Vesicle uptake was studied by confocal microscopy, as BPLVs were tagged with PE-rhodamine tracer (red signals), while cell nuclei with 4′,6-diamidino-2-phenylindole (DAPI; blue signals), and GPI-anchored proteins with Flaer-Alexa Fluor 488 (green signals). PBMCs were treated (w) or not (w/o) with BPLVs for 48 h and 72 h, and a baseline (T0) sample was used as control. PBMCs that have uptake BPLVs showed an intense merged purple signal, showing co-localization of PE-rhodamine vesicles and GPI-anchored proteins carried by BPLVs.

72 h; all $p > 0.05$). Whether to strengthen our hypothesis that BPLVs can deliver GPI-linked proteins to GPI-deficient cells, we studied Flaer expression on $BPLV^{-}$ populations, as we supposed that Flaer expression on those populations should not change over time because these cells did not uptake any extra GPI-anchored proteins. As expected, no significant variations were observed in Flaer expression on $BPLV^{-}$ cells in PNH, healthy controls, and samples treated with empty vesicles throughout the culture (all $p > 0.05$).

To investigate cellular mechanisms of BPLV uptake, a reversible clathrin inhibitor, Dyngo-4a, was used to block clathrin-mediated uptake in healthy and PNH PBMCs at 2 h, 5 h, and 12 h of culture without or with BPLVs (Figures 6E–6G). Cell membranes were stained with a lipophilic tracer (DiO), a green, fluorescent lipophilic carbocyanine dye emitting at 501 nm, that diffuses through plasma membrane and is widely used as an anterograde and retrograde neuronal tracer in living and fixed cells.[24] PE-rhodamine-conjugated BPLVs and DiO signals were investigated by confocal microscopy to visualize cellular uptake of vesicles (red signals) and co-localization on cell membranes (green signals) when Dyngo-4a was used (co-localization indicated by a merged orange signal). BPLV uptake block was observed at 2 h, 5 h, and 12 h in PNH PBMCs with vesicles mostly stacked on cell membranes, while in healthy PBMCs, merged signals were homogenously distributed, and lower amount of BPLVs were halted on cell surface.

GPI-anchored and not-GPI proteins are uptake by PBMCs

Next, we further investigated uptake and expression of both GPI-anchored and not-GPI proteins in PNH and healthy controls (Figure 7). PBMCs efficiently incorporated BPLVs, especially PNH cells with higher frequency of $BPLV^{+}CD3^{+}$ cells compared to healthy controls (mean ± SD, 10.31 ± 7.1% vs. 3.43 ± 1.8%; $p < 0.0001$), as well as $BPLV^{+}CD33^{+}$ cells (mean ± SD, 8.6 ± 6.6% vs. 2.56 ± 1.7%; p =

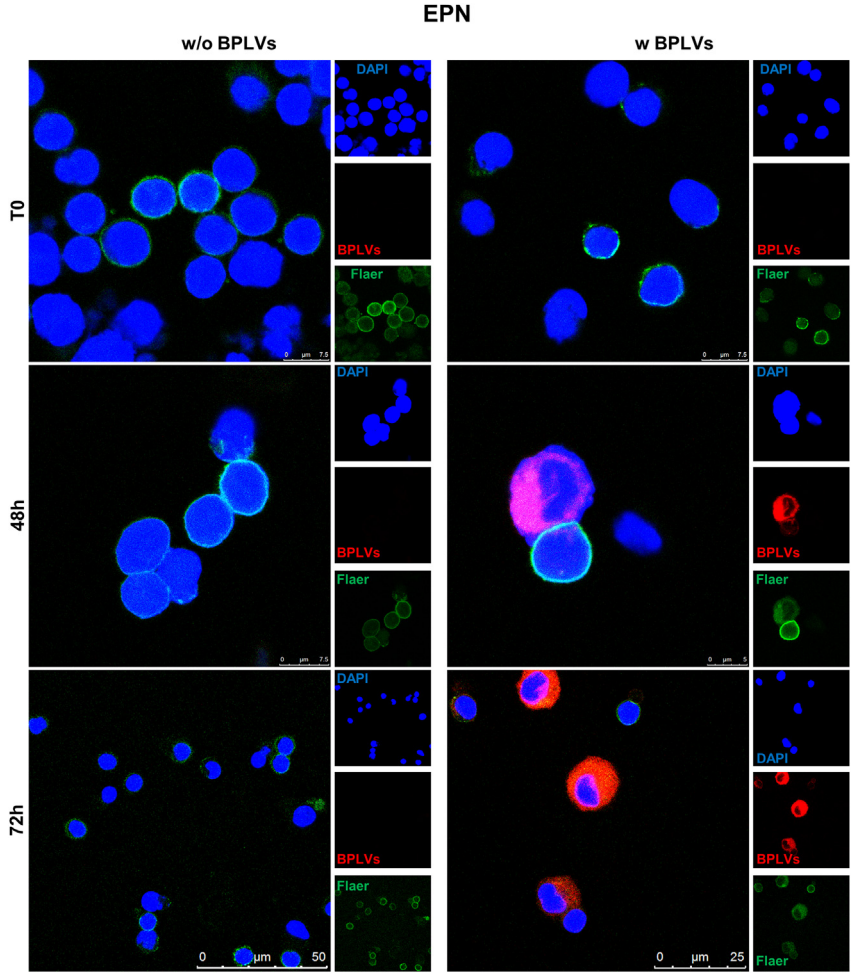

Figure 5. Biomimetic proteolipid vesicle (BPLV) uptake by paroxysmal nocturnal hemoglobinuria (PNH) peripheral blood mononuclear cells (PBMCs)
Vesicle uptake was studied by confocal microscopy, as BPLVs were tagged with PE-rhodamine tracer (red signals), while cell nuclei with 4′,6-diamidino-2-phenylindole (DAPI; blue signals), and GPI-anchored proteins with Flaer-Alexa Fluor 488 (green signals). PBMCs were treated (w) or not (w/o) with BPLVs for 48 h and 72 h, and a baseline (T0) sample was used as control. PBMCs that have uptake BPLVs showed an intense merged purple signal, showing co-localization of PE-rhodamine vesicles and GPI-anchored proteins carried by BPLVs.

0.0002) and BPLV$^+$HLA-DR$^+$ cells (mean ± SD, 6.82 ± 5.5% vs. 2.23 ± 1.5%; p = 0.0007), while BPLV$^+$CD14$^+$ cell frequency was similar between treated PNH and treated healthy control samples (mean ± SD, 2.3 ± 0.6% vs. 2.64 ± 1.6%; p = 0.7789).

Protein expression was also studied on BPLV$^+$ population, expressed as MFI values, and compared between time points for PNH, healthy controls, and samples treated with empty vesicles. No significant variations were observed for CD3 expression over culture time in all three groups (all p > 0.05), while CD33 expression was significantly increased at 72 h in PNH samples (mean MFI±SD, 23762 ± 11102 vs. 24054 ± 12707 vs. 35732 ± 11396, 24 h vs. 48 h vs. 72 h) compared to 24 h (p = 0.0244) and 48 h (p = 0.0058) of treatment. An increasing trend in CD14 (mean MFI±SD, 697 ± 531 vs. 1161 ± 891 vs. 1994 ± 1522, 24 h vs. 48 h vs. 72 h) and HLA-DR expression (mean MFI±SD, 3186 ± 2767 vs. 18819 ± 14116 vs. 95807 ± 71532, 24 h vs. 48 h vs. 72 h) was also observed. No significant variations or trends were observed in healthy controls and samples treated with empty vesicles over culture time for CD3, CD33, CD14, and HLA-DR (all p > 0.05), except for HLA-DR in healthy controls (mean MFI±SD, 1797 ± 394 vs. 15633 ± 5676 vs. 88147 ± 66437, 24 h vs. 48 h vs. 72 h; 24 h vs. 48 h, p = 0.0484 and 24 h vs. 72 h, p = 0.0812).

BPLVs increase cell resistance to complement-mediated lysis

Finally, to test the effects of BPLV treatment to increase the susceptibility to complement-mediated lysis on GPI-deficient cells, PNH cells were stressed with 10% FBS containing all complement components for 2 h and 24 h, and live and dead cell frequencies were assessed by flow cytometry (Figure 8). Samples were also treated with 10% decomplemented FBS, and untreated cells were used as controls. A ratio between dead and live cells in BPLV$^+$ and BPLV$^-$ populations was calculated, as cells more susceptible to lysis should display a higher ratio (dead

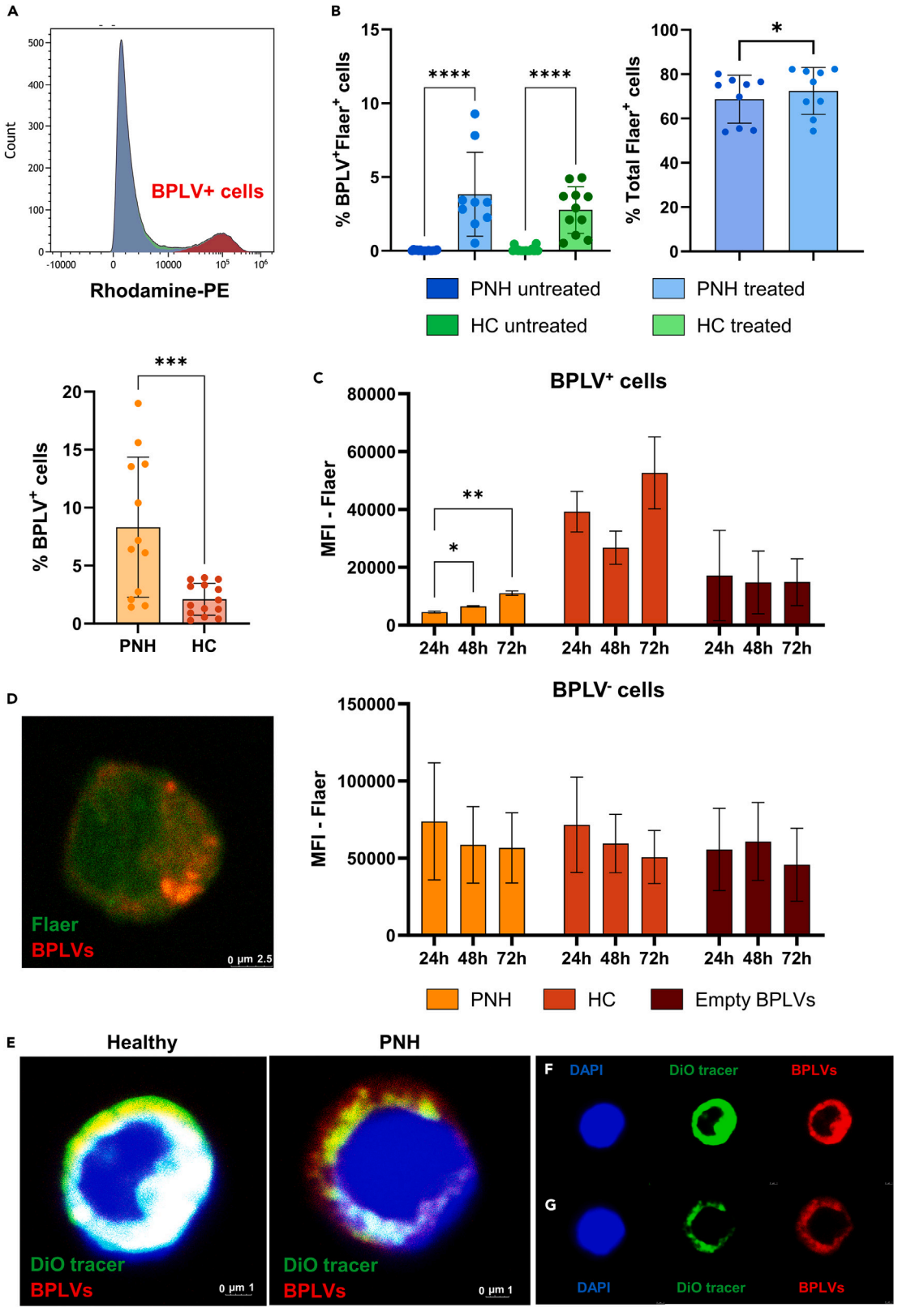
A
Count
BPLV+ cells
Rhodamine-PE
B
% BPLV+Flaer+ cells
****
****
% Total Flaer+ cells
*
PNH untreated
HC untreated
PNH treated
HC treated
***
% BPLV+ cells
PNH
HC
C
BPLV+ cells
MFI - Flaer
**
*
24h 48h 72h
BPLV- cells
D
Flaer
BPLVs
0 µm 2.5
PNH
HC
Empty BPLVs
E
Healthy
PNH
DiO tracer
BPLVs
0 µm 1
F
DAPI
DiO tracer
BPLVs
G

Figure 6. GPI-anchored protein expression by flow cytometry and cellular uptake

(A) Peripheral blood mononuclear cells were treated with biomimetic proteolipid vesicles (BPLVs) or empty (without proteins) nanocarriers for 24 h, 48 h, and 72 h, and those cells that have uptake the vesicles were identified as PE-rhodamine$^+$ population. Percentage of BPLV$^+$ cells in paroxysmal nocturnal hemoglobinuria (PNH) patients and healthy controls (HC) was calculated for cellular uptake.

(B) Flaer expression (GPI-anchored proteins) was studied on BPLV$^+$ cells, and percentage of BPLV$^+$Flaer$^+$ population or total Flaer$^+$ cells were indicated for untreated and treated PNH or HC group, as well (C) median fluorescence intensity (MFI) of Flaer expression on BPLV$^+$ or BPLV$^-$ populations were also reported. Data are represented as mean ± SD. *, $p < 0.05$; **, $p < 0.01$; ****, $p < 0.0001$.

(D) GPI-anchored proteins co-localization with PE-rhodamine BPLVs by confocal microscopy.

(E) Clathrin-dependent cellular mechanisms of vesicle uptake were investigated using a reversible clathrin inhibitor, Dyngo-4a, on healthy and PNH cells. Membranes were stained with a lipophilic tracer (DiO, green signal), while BPLVs were PE-conjugated (red signal), and merged signals for co-localization of vesicles on cell membranes are reported after 5 h of BPLV treatment in the presence of Dyngo-4a. Single channel images for (F) healthy and (G) PNH cells.

cells ≫ live cells), while cells more resistant to complement-mediated lysis a lower ratio (live cells ≫ dead cells). On lymphocytes and monocytes, both PNH and healthy control samples treated with BPLVs showed an increased resistance to complement-mediated lysis after normal and decomplemented FBS treatment (dead/live cell ratio, mean ± SD, 0.083 ± 0.07 and 0.090 ± 0.06, respectively) compared to untreated samples (dead/live cell ratio, mean ± SD, 1.02 ± 1.2 and 0.91 ± 1.03, after normal and decomplemented FBS treatment) (all $p < 0.05$). Similarly, treated granulocytes from both healthy and PNH samples displayed an increased resistance to complement-mediated lysis (dead/live cell ratio, mean ± SD, 0.72 ± 1.03 and 0.7 ± 0.9, after normal and decomplemented FBS treatment) compared to untreated cells (dead/live cell ratio, mean ± SD, 1.25 ± 1.3 and 1.5 ± 1.9, after normal and decomplemented FBS treatment), especially between cells treated with BPLVs with normal or decomplemented FBS and untreated cells stressed with normal FBS ($p = 0.0694$ and $p = 0.0499$, respectively).

PNH cell viability was also checked by MTT assay after treatment with 10% FBS containing or not all complement components for 24 h. When treated with complete FBS without previous treatment with BPLVs, cell viability decreased at 80%; however, this effect was reverted by adding BPLVs at 0.5 mg/mL, and cell viability significantly increased regardless the type of FBS used for lysis challenge ($p < 0.001$) (Figure 8E).

DISCUSSION

PNH, a benign clonal hematological condition within the BMF syndromes, is caused by a somatic mutation in the *PIGA* gene whose protein is involved in GPI anchor biosynthesis, and is characterized by a failure in membrane anchorage of proteins that require GPI-anchor to correctly localize on cell surface, including endogenous complement regulatory proteins CD55 and CD59.[25] Indeed, PNH symptoms are secondary to complement-induced cell lysis, such as intravascular RBC lysis and thrombosis, leading to anemia and thrombotic events.[26] Thromboembolism is the principal cause of mortality in PNH patients accounting for more than 40% of deaths, and can occur at any site, most commonly involving hepatic (Budd-Chiari syndrome, 7.5–25% of patients affected) and cerebral veins.[27] PNH symptoms are pharmacologically treated with complement inhibitors, to reduce complement activation on GPI-deficient cells thus improving their survival.[28] However, PNH clones accumulate into the peripheral blood and could be lysed during maximal complement activation (e.g., during bacterial infections), that overcomes complement inhibition, leading to breakthrough hemolysis, especially under novel complement inhibitor treatment, like ravulizumab.[29] Therefore, different pharmacological approaches are required to improve clinical management of PNH patients. Here, we formulated BPLVs carrying GPI-anchored proteins for an innovative therapeutic approach to obtain a new protein delivery system for reverting GPI deficiency in PNH cells.

BPLVs are hybrid synthetic vesicles produced by microfluidics methodologies by mixing an aqueous phase containing human membrane proteins derived from PBMCs and a lipid phase composed by different synthetic phospholipids at various concentrations,[18] and currently used for modulation of inflammatory processes.[18,21] In past decades, bioinspired delivery system development has been largely based on two strategies: bottom-up approaches, such as surface functionalization with antibodies mimicking cell surface proteins[21,30]; and top-down strategies, like cell-derived nanovesicles and nano-ghosts.[22] Conversely, recent microfluidics approaches allow the production of biomimetic vesicles that possess high surface complexity, versatility in formulations and payloads, standardized yield, and a stable, safe, and non-immunogenic product. BPLVs are nano-sized vesicles functionalized with human membrane proteins that have all the advantages of microfluidics-produced nanocarriers, and also retain tropism and functions of leukocytes, such as *trans*-endothelial migration, modulation and resolution of inflammation.[18–21] Here, we applied this platform for an innovative protein delivery, as we engineered a nanocarrier system capable to deliver to cells GPI-anchored proteins without altering cell genome, while just delivering missing molecules using this biomimetic platform. Other formulations and process parameters, such as ethanol/water ratios and flow rates, were also optimized to produce monodispersed unilamellar BPLV batches using a microfluidic technology. Indeed, in our formulation design, water and lipid phases were mixed using a NanoGenerator Flex M microfluidic platform with a Y-shaped micrometer cartridge with an overall length of 10 cm (internal diameter, 0.6 μm), different from a previously described approach for leucosome formulation.[20,21] This apparatus could also fabricate large amounts of products in shorter time, because of the higher flow rate adopted (4 mL/min) compared to previously reported (1 mL/min).[21] Furthermore, our chosen protein:lipid ratio (1:35) assured an excellent protein loading. Therefore, our formulation showed a great potential of scale-up protocol combined with good loading and product stability, extremely important for large scale *in vitro* and *in vivo* studies.

RBCs and PBMCs treated with BPLVs showed an excellent uptake with membrane exposure of GPI-anchored proteins, suggesting that adopted fabrication protocol did not alter post-translational modifications of proteins that were successfully incorporated within lipid

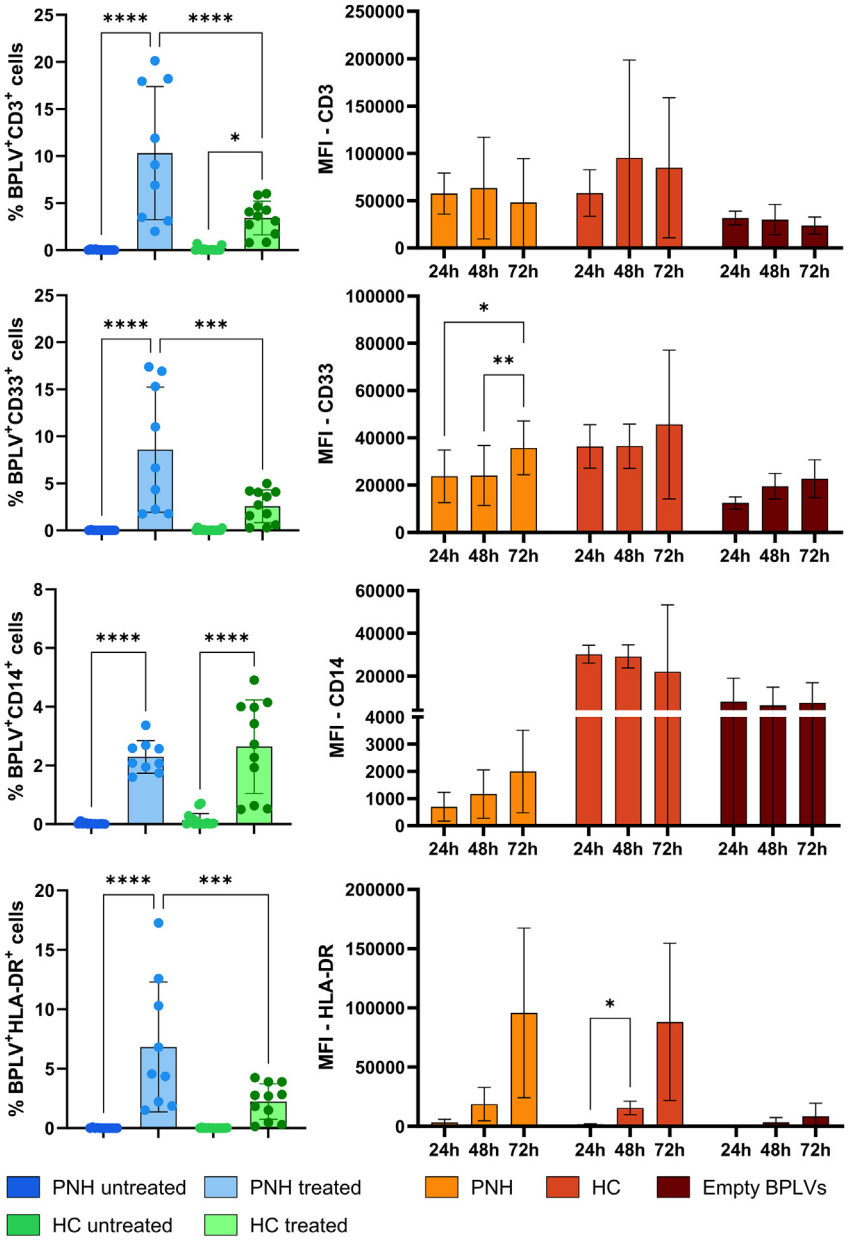

Figure 7. GPI-anchored and not-GPI protein expression by flow cytometry

Peripheral blood mononuclear cells were treated with biomimetic proteolipid vesicles (BPLVs) or empty (without proteins) nanocarriers for 24 h, 48 h, and 72 h, and those cells that have uptake the vesicles were identified as PE-rhodamine^{+} population. On BPLV^{+} cells, CD14 (GPI-anchored protein), CD3, CD33, and HLA-DR (all not-GPI proteins) expression was studied, as well median fluorescence intensity (MFI) of each studied marker was also reported. Data are represented as mean ± SD. *, $p < 0.05$; **, $p < 0.01$; ***, $p < 0.001$; ****, $p < 0.0001$.

bilayers, and vesicles were efficiently uptaken by cells. In particular, BPLVs were observed homogenously distributed within cytoplasm and cell membrane, with some accumulations within intracytoplasmic vacuoles, likely endosomes, suggesting that BPLVs were internalized by cells through an active transport. Indeed, PNH and healthy control cells displayed a different behavior in vesicle uptake, with GPI-deficient cells more prone to incorporate synthetic vesicles (empty BPLVs). Previous studies have described endocytosis defects of PNH cells linked to unstable lipid rafts, because of the lack of GPI-anchored proteins that stabilize those rafts, and to reduced caveolae-mediated internalization.[30] However, GPI-anchored proteins have distinct endocytosis mechanisms that differ from other regular cellular endocytic pathways, such as clathrin-coated pits (caveolae)-mediated, and depends on lateral associations of GPI-linked proteins with cholesterol and sphingolipids at the exoplasmic leaflet of plasma membrane, resulting in a very quick (2 min) membrane invagination, known as GPI-anchored protein enriched endosomal compartments.[31] These mechanisms could explain the increased ability of PNH cells to uptake BPLVs and to incorporate

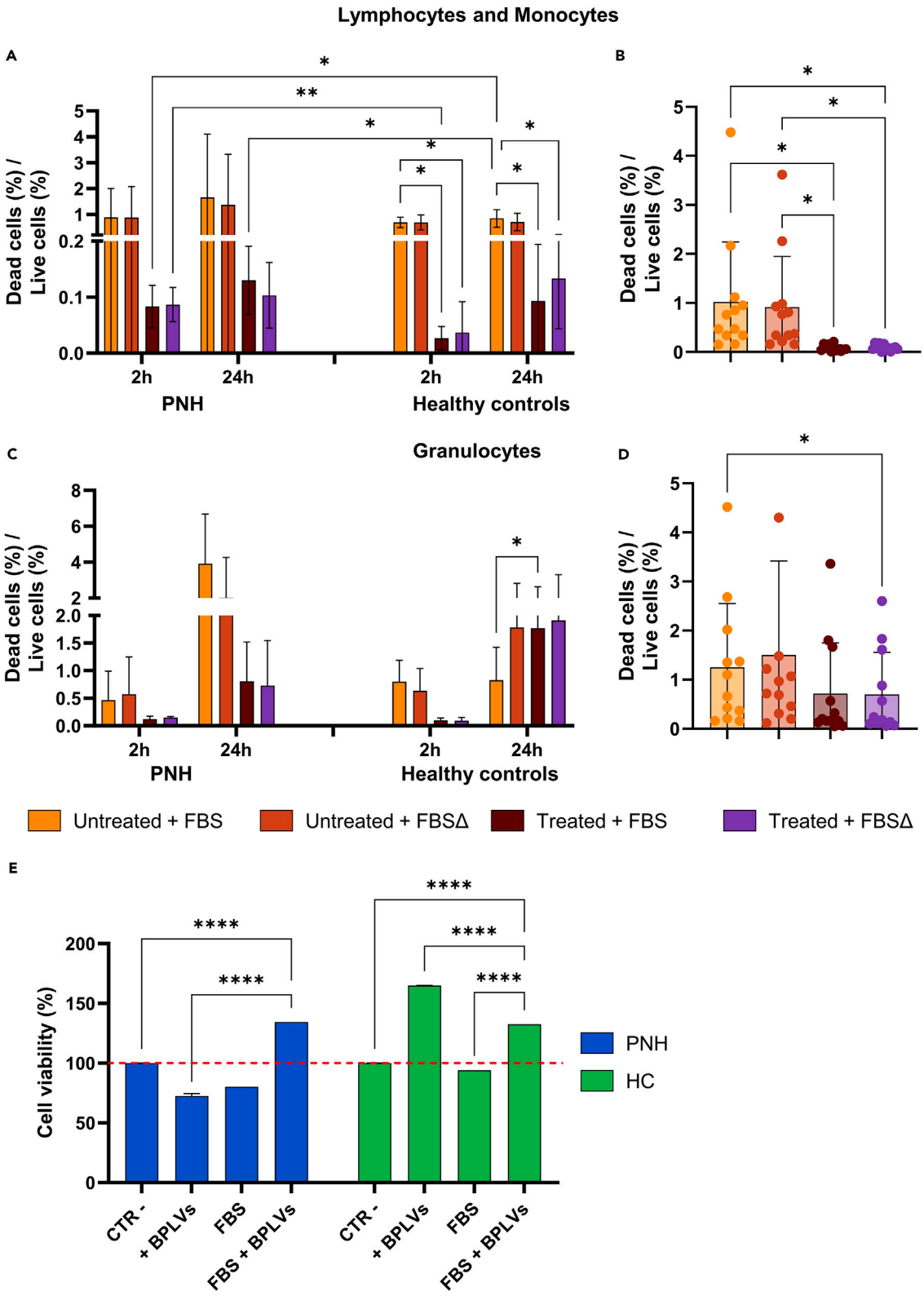

Figure 8. ***In vitro*** **lysis test**

To test resistance to complement-mediated lysis after biomimetic proteolipid vesicle (BPLV) treatment, peripheral blood mononuclear cells (PBMCs) from healthy controls (HC) and paroxysmal nocturnal hemoglobinuria (PNH) patients were first incubated without or with BPLVs using a culture medium

Figure 8. *Continued*

supplemented with 10% of decomplemented fetal bovine serum (FBS). Subsequently, culture medium was replaced with fresh medium containing 10% decomplemented (Δ) or normal FBS, and cells were incubated for 2 h or 24 h, and then cell viability tested by (A–D) flow cytometry and (E) MTT assay. $BPLV^+$ live and $BPLV^+$ dead cells, or $BPLV^-$ live and $BPLV^-$ dead cells were identified, and a ratio between dead and live cells in each population was calculated.
(A) Cell viability by flow cytometry in HC and PNH lymphocytes and monocytes, or (B) in total samples (HC + PNH) compared by treatments.
(C) Cell viability by flow cytometry in HC and PNH granulocytes, or (D) in total samples (HC + PNH) compared by treatments. Data are represented as mean ± SD.
*, $p < 0.05$; **, $p < 0.01$; ****, $p < 0.0001$.

and recycle GPI-linked proteins on cell surface, with a significant reduction of PNH clone size just after 72 h of treatment. Moreover, when clathrin-mediated internalization was blocked, BPLVs stacked on surface of PNH cells, while not of healthy PBMCs.

Peripheral blood cells displayed an increased resistance to complement-mediated lysis after BPLV treatment, although their disruption is not directly involved in PNH symptoms development (anemia and thrombosis). However, several studies have described impairment in lymphocyte and monocyte functions in PNH patients, such as increased exhaustion of effector memory $CD8^+$ T cells and ineffective dendritic cell maturation of GPI-deficient monocytes after *in vitro* stimulation.[32,33] Moreover, granulocytes also display dysregulated functions, such as impaired migration abilities, higher pro-inflammatory activities, and likely an increased susceptibility to release granules.[34] Therefore, hemolysis and thrombosis might be only the tip of the iceberg, as impaired immune responses could concur to increase the risk of life-threating infections during complement inhibition therapy, as cells are not lysed while their functions might still be altered.[35] GPI-defective T lymphocytes show severe defects in T cell receptor-dependent proliferation, CD25, CD54, and HLA-DR surface expression, molecule activation, and cytokine production, also due to altered signaling transduction.[36] Indeed, GPI-anchored proteins are not only surface proteins, but also inner leaflet-signaling transducers, such as Src-related tyrosine kinases, and PNH cells might defect in coupling events for intracellular signaling pathways.[37,38] Moreover, PNH patients show persistence of Fas-ligand on lymphocytes and granulocytes with increased resistance to cytokine-induced apoptosis.[36–38] These mechanisms might concur to PNH symptom development and disease pathophysiology; therefore, improvement of resistance to complement-mediated lysis not only of RBCs, but also of all peripheral blood cells might significantly ameliorate clinical manifestations. Indeed, we showed that BPLV-treated cells from PNH and healthy subjects had increased expression of HLA-DR, that might restore normal T cell functions, and of all surface GPI-anchored proteins, augmenting resistance to complement-mediated lysis. In addition, it is plausible that treated cells might have uptake also inner leaflet-GPI proteins; however, further *in vitro* studies are required to elucidate changes in lymphocyte and granulocyte functions after BPLV treatment.

In conclusion, we provided an innovative approach for treatment of PNH-related symptoms with the use of hybrid and semi-synthetic nanocarriers, composed by human membrane proteins and synthetic phospholipids, as a protein delivery system for release of the entire set of GPI-anchored proteins to PNH cells without altering cell genome. To the best of our knowledge, this approach represents an innovation in the PNH field, as this protein delivery platform produced by incorporation of complex protein extracts into lipid vesicles using a microfluidic technology has been used for delivering deficient proteins in PNH cells. Our vesicles are biomimetic, not toxic, and extremely affine to cell membrane resulting in an excellent uptake and protein delivery that could efficiently revert protein deficiency in PNH clones. Our results open new therapeutic scenarios, as cell phenotype was modified without introducing changes in the DNA, thus overcoming all technical issues related to the use of viral vectors or other genome modifiers. These modifications are likely transient, because they rely on cell lifespan, as we did not introduce permanent modifications in cell genome. This aspect could be a disadvantage, as patients might require prolonged treatments; conversely, treatment-related adverse events might be better managed by dose and time modulation. Our system could be further used for incorporation of chimeric receptors or other recombinant proteins within nanocarriers for advanced drug-delivery functions and treatment of a broad range of disorders caused by specific protein deficiency. Despite our results are very promising and encouraging, further validation in additional *in vitro* and *in vivo* studies are required.

Limitations of the study

Limitations of our work are: first, lack of *in vivo* studies, because current mouse models cannot efficiently reproduce clinical PNH manifestations, such as hemolysis and thrombosis.[39] Conventional *Pig-A* knockout mouse models frequently results in a high rate fetal death and low chimeric rate (<5%) of PNH clone in born mice, likely because *Pig-A* is a key gene in embryonic mouse development.[40] Moreover, these PNH clones significantly reduce after birth and cannot reproduce PNH clonal proliferation;[41] second, the small number of patients, because of the rarity of studied disease without accompanying aplastic anemia (0.35 cases per 100,000 people);[42] and third, lack of RBC lysis test, because there are no specific assays for identification of complement-mediated hemolysis and because there are no standardized protocols for long-term mature RBC culture.[43,44] On the other hand, lack of *in vivo* pharmacokinetics studies to investigate blood circulation behaviors of BPLVs; however, biomimetic vesicles should possess 5-fold longer circulation time compared to liposomes, as previously reported.[18]

STAR★METHODS

Detailed methods are provided in the online version of this paper and include the following:

- KEY RESOURCES TABLE
- RESOURCE AVAILABILITY
  - Lead contact
  - Materials availability

ACKNOWLEDGMENTS

The Authors would like to thank the Flow Cytometry Core (University Hospital "San Giovanni di Dio e Ruggi d'Aragona", Salerno, Italy), and Dr. Letizia D'Apice (Beckman Coulter, Milan, Italy).

This research was supported by the Intramural Program of the Department of Medicine, Surgery and Dentistry, University of Salerno, Italy (FARB 2021 Della Porta and FARB 2021 Selleri).

AUTHOR CONTRIBUTIONS

Conceptualization, V.G., G.D.P., and C.S.; formulation, P.S. and E.P.L.; methodology, G.D.P., V.G., P.S., E.P.L., M.G., A.B., and F.P.; clinical data, B.S.; writing – original draft preparation, V.G. and P.S.; writing – review and editing, G.D.P. and C.S. All authors have read and agreed to the published version of the manuscript.

DECLARATION OF INTERESTS

The Authors V.G., P.S., E.P.L., G.D.P., and C.S. disclose a patent no. 102023000015003 (18/07/2023).

Received: October 20, 2023
Revised: December 26, 2023
Accepted: January 22, 2024
Published: January 25, 2024

REFERENCES

1. Patel, B.A., Giudice, V., and Young, N.S. (2021). Immunologic effects on the haematopoietic stem cell in marrow failure. Best Pract. Res. Clin. Haematol. *34*, 101276.
2. Giudice, V., and Selleri, C. (2022). Aplastic anemia: Pathophysiology. Semin. Hematol. *59*, 13–20.
3. Giudice, V., Risitano, A.M., and Selleri, C. (2021). Infectious Agents and Bone Marrow Failure: A Causal or a Casual Connection? Front. Med. *8*, 757730.
4. Risitano, A.M., Peffault de Latour, R., Marano, L., and Frieri, C. (2022). Discovering C3 targeting therapies for paroxysmal nocturnal hemoglobinuria: Achievements and pitfalls. Semin. Immunol. *59*, 101618.
5. Risitano, A.M., Frieri, C., Urciuoli, E., and Marano, L. (2023). The complement alternative pathway in paroxysmal nocturnal hemoglobinuria: From a pathogenic mechanism to a therapeutic target. Immunol. Rev. *313*, 262–278.
6. Shah, S., Dhawan, V., Holm, R., Nagarsenker, M.S., and Perrie, Y. (2020). Liposomes: Advancements and innovation in the manufacturing process. Adv. Drug Deliv. Rev. *154–155*, 102–122.
7. Campardelli, R., Espirito Santo, I., Albuquerque, E.C., de Melo, S.V., Della Porta, G., and Reverchon, E. (2016). Efficient encapsulation of proteins in submicro liposomes using a supercritical fluid assisted continuous process. J. Supercrit. Fluids *107*, 163–169.
8. Espirito Santo, I., Campardelli, R., Albuquerque, E.C., de Melo, S.V., Della Porta, G., and Reverchon, E. (2014). Liposomes preparation using a supercritical fluid assisted continuous process. Chem. Eng. J. *249*, 153–159.
9. Lamparelli, E.P., Ciardulli, M.C., Scala, P., Scognamiglio, M., Charlier, B., Di Pietro, P., Izzo, V., Vecchione, C., Maffulli, N., and Della Porta, G. (2022). Lipid nano-vesicles for thyroid hormone encapsulation: A comparison between different fabrication technologies, drug loading, and an *in vitro* delivery to human tendon stem/progenitor cells in 2D and 3D culture. Int. J. Pharm. *624*, 122007.
10. Yu, B., Lee, R.J., and Lee, L.J. (2009). Microfluidic methods for production of liposomes. Methods Enzymol. *465*, 129–141.
11. Liu, Y., Yang, G., Hui, Y., Ranaweera, S., and Zhao, C.X. (2022). Microfluidic Nanoparticles for Drug Delivery. Small *18*, e2106580.
12. Heurtault, B., Saulnier, P., Pech, B., Proust, J.E., and Benoit, J.P. (2003). Physico-chemical stability of colloidal lipid particles. Biomaterials *24*, 4283–4300.
13. Tenchov, R., Bird, R., Curtze, A.E., and Zhou, Q. (2021). Lipid Nanoparticles—From Liposomes to mRNA Vaccine Delivery, a Landscape of Research Diversity and Advancement. ACS Nano *15*, 16982–17015.

14. Hou, X., Zaks, T., Langer, R., and Dong, Y. (2021). Lipid nanoparticles for mRNA delivery. Nat. Rev. Mater. *6*, 1078–1094.
15. Behzadi, S., Serpooshan, V., Tao, W., Hamaly, M.A., Alkawareek, M.Y., Dreaden, E.C., Brown, D., Alkilany, A.M., Farokhzad, O.C., and Mahmoudi, M. (2017). Cellular uptake of nanoparticles: journey inside the cell. Chem. Soc. Rev. *46*, 4218–4244.
16. Alexis, F., Pridgen, E., Molnar, L.K., and Farokhzad, O.C. (2008). Factors affecting the clearance and biodistribution of polymeric nanoparticles. Mol. Pharm. *5*, 505–515.
17. Robbins, G.P., Saunders, R.L., Haun, J.B., Rawson, J., Therien, M.J., and Hammer, D.A. (2010). Tunable leuko-polymersomes that adhere specifically to inflammatory markers. Langmuir *26*, 14089–14096.
18. Molinaro, R., Corbo, C., Martinez, J.O., Taraballi, F., Evangelopoulos, M., Minardi, S., Yazdi, I.K., Zhao, P., De Rosa, E., Sherman, M.B., et al. (2016). Biomimetic proteolipid vesicles for targeting inflamed tissues. Nat. Mater. *15*, 1037–1046.
19. Martinez, J.O., Molinaro, R., Hartman, K.A., Boada, C., Sukhovershin, R., De Rosa, E., Kirui, D., Zhang, S., Evangelopoulos, M., Carter, A.M., et al. (2018). Biomimetic nanoparticles with enhanced affinity towards activated endothelium as versatile tools for theranostic drug delivery. Theranostics *8*, 1131–1145.
20. Molinaro, R., Evangelopoulos, M., Hoffman, J.R., Corbo, C., Taraballi, F., Martinez, J.O., Hartman, K.A., Cosco, D., Costa, G., Romeo, I., et al. (2018). Design and Development of Biomimetic Nanovesicles Using a Microfluidic Approach. Adv. Mater. *30*, e1702749.
21. Zinger, A., Sushnitha, M., Naoi, T., Baudo, G., De Rosa, E., Chang, J., Tasciotti, E., and Taraballi, F. (2021). Enhancing Inflammation Targeting Using Tunable Leukocyte-Based Biomimetic Nanoparticles. ACS Nano *15*, 6326–6339.
22. Cançado, R.D., Araújo, A.D.S., Sandes, A.F., Arrais, C., Lobo, C.L.D.C., Figueiredo, M.S., Gualandro, S.F.M., Saad, S.T.O., and Costa, F.F. (2021). Consensus statement for diagnosis and treatment of paroxysmal nocturnal haemoglobinuria. Hematol. Transfus. Cell Ther. *43*, 341–348.
23. Sutherland, D.R., Kuek, N., Davidson, J., Barth, D., Chang, H., Yeo, E., Bamford, S., Chin-Yee, I., and Keeney, M. (2007). Diagnosing PNH with FLAER and multiparameter flow cytometry. Cytometry B Clin. Cytom. *72*, 167–177.
24. Fritzsch, B., Muirhead, K.A., Feng, F., Gray, B.D., and Ohlsson-Wilhelm, B.M. (2005). Diffusion and imaging properties of three new lipophilic tracers, NeuroVue Maroon, NeuroVue Red and NeuroVue Green and their use for double and triple labeling of neuronal profile. Brain Res. Bull. *66*, 249–258.
25. Peffault de Latour, R., and Risitano, A.M. (2023). Complement inhibition in medicine: Hematology and beyond; complement inhibition in hematology: PNH and beyond. Am. J. Hematol. *98*, S3–S4.
26. Chatzileontiadou, S., Hatjiharissi, E., Angelopoulou, M., Asimakopoulos, J.V., Loutsidi, N.E., Chatzikonstantinou, T., Zikos, P., Bouchla, A., Bezirgiannidou, Z., Kouvata, E., et al. (2023). Thromboembolic events in patients with paroxysmal nocturnal hemoglobinuria (PNH): Real world data of a Greek nationwide multicenter retrospective study. Front. Oncol. *13*, 1128994.
27. Hill, A., Kelly, R.J., and Hillmen, P. (2013). Thrombosis in paroxysmal nocturnal hemoglobinuria. Blood *121*, 4985–5105.
28. Frieri, C., Peffault de Latour, R., and Sicre De Fontbrune, F. (2022). Emerging drugs for the treatment of paroxysmal nocturnal hemoglobinuria. Expert Opin. Emerg. Drugs *27*, 33–43.
29. Notaro, R., and Luzzatto, L. (2022). Breakthrough Hemolysis in PNH with Proximal or Terminal Complement Inhibition. N. Engl. J. Med. *387*, 160–166.
30. Zeng, L., Liu, H., Liu, Z., Li, L., Wang, H., Chen, Y., Wu, J., Wang, G., Li, L., and Fu, R. (2023). Defected lipid rafts suppress cavin1-dependent IFN-α signaling endosome in paroxysmal nocturnal hemoglobinuria. Int. Immunopharmacol. *115*, 109468.
31. Lakhan, S.E., Sabharanjak, S., and De, A. (2009). Endocytosis of glycosylphosphatidylinositol-anchored proteins. J. Biomed. Sci. *16*, 93.
32. Hosokawa, K., Kajigaya, S., Keyvanfar, K., Qiao, W., Xie, Y., Townsley, D.M., Feng, X., and Young, N.S. (2017). T Cell Transcriptomes from Paroxysmal Nocturnal Hemoglobinuria Patients Reveal Novel Signaling Pathways. J. Immunol. *199*, 477–488.
33. Ruggiero, G., Terrazzano, G., Becchimanzi, C., Sica, M., Andretta, C., Masci, A.M., Racioppi, L., Rotoli, B., Zappacosta, S., and Alfinito, F. (2004). GPI-defective monocytes from paroxysmal nocturnal hemoglobinuria patients show impaired *in vitro* dendritic cell differentiation. J. Leukoc. Biol. *76*, 634–640.
34. Hosokawa, K., Kajigaya, S., Keyvanfar, K., Qiao, W., Xie, Y., Biancotto, A., Townsley, D.M., Feng, X., and Young, N.S. (2017). Whole transcriptome sequencing identifies increased CXCR2 expression in PNH granulocytes. Br. J. Haematol. *177*, 136–141.
35. Li, C., Dong, X., Wang, H., and Shao, Z. (2021). The Role of T Lymphocytes in the Pathogenesis of Paroxysmal Nocturnal Hemoglobinuria. Front. Immunol. *12*, 777649.
36. Terrazzano, G., Sica, M., Becchimanzi, C., Costantini, S., Rotoli, B., Zappacosta, S., Alfinito, F., and Ruggiero, G. (2005). T cells from paroxysmal nocturnal haemoglobinuria (PNH) patients show an altered CD40-dependent pathway. J. Leukoc. Biol. *78*, 27–36.
37. Horejsí, V., Drbal, K., Cebecauer, M., Cerný, J., Brdicka, T., Angelisová, P., and Stockinger, H. (1999). GPI-microdomains: a role in signalling via immunoreceptors. Immunol. Today *20*, 356–361.
38. Kunyaboon, R., Wanachiwanawin, W., U-Pratya, Y., Thedsawad, A., and Taka, O. (2012). Mechanism of paroxysmal nocturnal hemoglobinuria clonal dominance: possible roles of different apoptosis and CD8+ lymphocytes in the selection of paroxysmal nocturnal hemoglobinuria clones. Hematol. Oncol. Stem Cell Ther. *5*, 138–145.
39. Chen, Y., and Rong, F. (2021). Advances in the creation of animal models of paroxysmal nocturnal hemoglobinuria. Hematology *26*, 491–496.
40. Murakami, Y., and Kinoshita, T. (2017). Animal Models of Paroxysmal Nocturnal Hemoglobinuria. In Paroxysmal Nocturnal Hemoglobinuria, Y. Kanakura, T. Kinoshita, and J. Nishimura, eds. (Springer). https://doi.org/10.1007/978-4-431-56003-6_3.
41. Rosti, V., Tremml, G., Soares, V., Pandolfi, P.P., Luzzatto, L., and Bessler, M. (1997). Murine embryonic stem cells without pig-a gene activity are competent for hematopoiesis with the PNH phenotype but not for clonal expansion. J. Clin. Invest. *100*, 1028–1036.
42. Richards, S.J., Painter, D., Dickinson, A.J., Griffin, M., Munir, T., Arnold, L., Payne, D., Pike, A., Muus, P., Hill, A., et al. (2021). The incidence and prevalence of patients with paroxysmal nocturnal haemoglobinuria and aplastic anaemia PNH syndrome: A retrospective analysis of the UK's population-based haematological malignancy research network 2004-2018. Eur. J. Haematol. *107*, 211–218.
43. Gupta, R., Pandey, P., Choudhry, R., Kashyap, R., Mehrotra, M., Naseem, S., and Nityanand, S. (2007). A prospective comparison of four techniques for diagnosis of paroxysmal nocturnal hemoglobinuria. Int. J. Lab. Hematol. *29*, 119–126.
44. Risso, A., Ciana, A., Achilli, C., and Minetti, G. (2014). Survival and senescence of human young red cells *in vitro*. Cell. Physiol. Biochem. *34*, 1038–1049.
45. Sposini, S., Jean-Alphonse, F.G., Ayoub, M.A., Oqua, A., West, C., Lavery, S., Brosens, J.J., Reiter, E., and Hanyaloglu, A.C. (2017). Integration of GPCR Signaling and Sorting from Very Early Endosomes via Opposing APPL1 Mechanisms. Cell Rep. *21*, 2855–2867.

STAR★METHODS

KEY RESOURCES TABLE

REAGENT or RESOURCE	SOURCE	IDENTIFIER
Antibodies		
FLAER-AlexaFluor 488	Euroclone	FL1SC
CD3-ECD – clone UCHT1	Beckman Coulter	Cat.no.A07748; RRID:AB_1575956
CD33-PC5.5 – clone D3HL60.251	Beckman Coulter	Cat.no.B36289
CD14-Alexa Fluor 750 – clone RMO52	Beckman Coulter	Cat.no.B92421; RRID:AB_2909815
CD45-Krome Orange – clone J.33	Beckman Coulter	Cat.no.B36294; RRID:AB_2833027
HLA-DR-SuperNova 780 – clone Immu-357	Beckman Coulter	Cat.no.C78087
Biological samples		
Healthy peripheral blood mononuclear cells	Human, Peripheral blood	Caucasian, M/F, 2/4; mean age, 34 years old; range, 23-45 years old
PNH peripheral blood mononuclear cells	Human, Peripheral blood	Caucasian, M/F, 1/2; mean age, 63 years old; range, 16-87 years old
Chemicals, peptides, and recombinant proteins		
1,2-dipalmitoyl-sn-glycero-3-phosphocholine (DPPC)	Avanti polar lipids Inc	Cat.no.850355P
1,2-dioleoyl-sn-glycero-3-phosphocholine (DOPC)	Avanti polar lipids Inc	Cat.no.850375P
Cholesterol	Avanti polar lipids Inc	Cat.no. 700000
1,2-dioleoyl-sn-glycero-3-phosphoethanolamine-N-lissamine rhodamine B sulfonyl (Liss Rhod PE)	Avanti polar lipids Inc	Cat.no. 810150
Ficoll-paque density gradient media	Cytiva	Cat.no. 17144002
Phosphotungstic acid solution 2%	Ted Pella Inc.	Cat.no. 19402
3-(4,5-Dimethylthiazol-2-yl)-2,5-diphenyl-tetrazolium bromide (MTT)	Sigma-Aldrich	CAS No.298-93-1
4′,6-diamidino-2-phenylindole (DAPI)	Sigma-Aldrich	CAS No.28718-3
Clathrin/dynamin inhibitor Dyngo-4	Abcam	Cat.no.ab120689
Fixable Viability Dye eFluor™ 780	eBioscience™	Cat.no. 47-4317-82; RRID:AB_10366688
Critical commercial assays		
ProteoExtract native membrane protein extraction kit	Sigma-Aldrich	Cat.no. 444810-1KIT
Bradford assay	BioRad	Cat.no. 5000006
Dialysis tubing benzoylated	Sigma-Aldrich	Cat.no. D7884
Vybrant DiO cell labeling solution	Thermo Fisher Scientific	Cat.no. V22886
Software and algorithms		
ImageJ software v.1.54b	NIH	https://imagej.nih.gov/ij/; RRID:SCR_003070
FlowJo software v.10.8.1	BD Biosciences	https://www.flowjo.com/solutions/flowjo; RRID:SCR_008520
Kaluza Analysis Flow Cytometry Software v2.1.1	Beckman Coulter	https://www.beckman.it/flow-cytometry/software/kaluza/downloads; RRID:SCR_016182

(*Continued on next page*)

Continued

REAGENT or RESOURCE	SOURCE	IDENTIFIER
Other		
NanoGenerator Flex M for NanoParticle Synthesis	Precigenome	SKU: PG-SYN-F
Microfluidic Mixer Chip MIX-3 for NanoParticle Synthesis	Precigenome	SKU: CHP-MIX-3

RESOURCE AVAILABILITY

Lead contact

Further information and requests for resources and reagents should be directed to and will be fulfilled by the lead contact, Giovanna Della Porta (gdellaporta@unisa.it).

Materials availability

This study did not generate new unique reagents.

Data and code availability

- Data: Data reported in this paper will be shared by the lead contact upon request.
- Code: This paper does not report original code.
- All other requests: Any additional information required to reanalyze the data reported will be shared by the lead contact upon request.

EXPERIMENTAL MODEL AND STUDY PARTICIPANT DETAILS

Subjects

A total of 3 (Caucasian, M/F, 1/2; mean age, 63 years old; range, 16-87 years old) consecutive PNH patients were included in this study. Diagnosis was made based on current international guidelines [22], between November 2022 and February 2023 at the Hematology and Transplant Center, University Hospital "San Giovanni di Dio e Ruggi d'Aragona", Salerno, Italy. All patients were eculizumab-resistant and ravulizumab was initiated in all subjects. Mean PNH clone size at study enrollment was 86.9% (range, 74.9-100%). Whole heparinized peripheral blood (PB) specimens were collected under ravulizumab treatment in accordance with the Declaration of Helsinki and protocols approved by local Ethic Committee "Campania Sud" (Brusciano, Naples, Italy; prot./SCCE n. 24988). A total of six healthy subjects (Caucasian, M/F, 2/4; mean age, 34 years old; range, 23-45 years old) was enrolled for protein extraction and for functional studies. Peripheral blood mononuclear cells (PBMCs) were isolated by Ficoll-Paque gradient centrifugation, and cells were stored in RPMI (Gibco™, Waltham, Massachusetts, USA) supplemented with 20% of decomplemented FBS (Gibco™) and 10% of dimethyl sulfoxide (DMSO; Sigma Aldrich, Milan, Italy) at -80°C until use.

Ethical approval

Protocol approved by local ethic committee (Ethics Committee "Campania Sud", Brusciano, Naples, Italy; prot./SCCE n. 24988).

Informed consent

Patients received informed consent obtained in accordance with the Declaration of Helsinki (World Medical Association 2013) and protocols approved by local ethic committee (Ethics Committee "Campania Sud", Brusciano, Naples, Italy; prot./SCCE n. 24988).

METHOD DETAILS

Membrane protein extraction and quantification

PBMCs were isolated from whole peripheral blood of healthy donors through Ficoll-paque density gradient centrifugation (Cytiva, Marlborough, Massachusetts, United States). $5x10^6$ PBMCs were employed to extract membrane proteins using ProteoExtract native membrane protein extraction kit (Sigma-Aldrich). Extracted protein concentration was quantified by Bradford assay (BioRad), absorbance was measured at 480 nm with microplate reader (Infinite F200 PRO, Tecan Group Ltd., SW) and frozen at -80°C till use.

BPLV preparation

BPLVs were produced by microfluidic technique using the NanoGenerator Flex M (Precigenome LLC San Jose, CA- USA), equipped with a passive staggered herringbone microchip. The organic phase was composed of 1,2-dipalmitoyl-sn-glycero-3-phosphocholine (DPPC), 1,2-dioleoyl-sn-glycero-3-phosphocholine (DOPC), cholesterol, and Liss Rhod PE solubilized in ethanol at 8 mg/mL, 6.4 mg/mL, 3.1 mg/mL, and

1 mg/mL respectively (see also patent no. 102023000015003), and sonicated at 45°C for 5 minutes. All lipid components are from Avanti polar lipids Inc., Alabaster, Alabama, US. Water phase was composed of only Milli-Q water for empty BPLVs and Milli-Q water plus PBMC-derived membrane proteins at 0.5mg/mL, protein:lipid ratio (1:35) for loaded BPLVs. Lipid and water phases were injected within a Y-shaped microfluidic cartridge at constant Flow Rate Ratio (FRR) 1:2 (ethanol/water) and adapting the Total Flow Rate (TFR) 4 mL/min. Then, 5mL of each BPLV formulation was dialyzed in 500 mL of Milli-Q water using a 2000 NMWCO Dialysis tubing benzoylated (Sigma-Aldrich) under a gentle stirrer at room temperature overnight.

BPLV characterization

BPLV size, distribution, and ζ-potential were measured by dynamic light scattering (DLS) by Nano ZS Malvern Zeta Sizer (model 1000HSa, UK) at 25°C equipped with a He-Ne laser of 633 nm and a detector angle of 173°C. BPLV size and concentration was also evaluated using a NanoSight NS300 (Malvern Panalytical, Westbourough MA) just after production and after 1 month to evaluate their stability stored at +4°C. All measurements were conducted in triplicate for empty and loaded BPLVs.

Nano-vesicles morphology was observed by Transmission electron microscope (TEM) FEI TECNAI G2 200 kV S-TWIN microscope equipped with a 4 K camera (electron source with LaB6 emitter; FEI Company, Dawson Creek Drive, Hillsboro, OR, USA). Briefly, 8 μL of diluted BPLV suspension was applied in a formvar/carbon 200 mesh copper grid (Ted Pella, USA Cat.No.01800-F) and dried for several hours. Subsequently, specimens were stained with phosphotungstic acid solution (2% w/v) directly made on the deposit for 60 s, and then air-dried overnight. TEM micrographs in brightfield modes were taken by Brightfield (BF) TEM images were acquired at 120 kV using a spot size of 3, and an integration time of 1 s. ImageJ software (v.1.54b; National Institutes of Health, Bethesda, MD, USA) was used for image analysis and rescaling.

BPLV flow cytometry

For PE-BPLV characterization, vesicles were resuspended in 100 μL of filtered water and stained with FLAER-AlexaFluor 488, CD3-ECD, CD33-PC5.5, CD14-Alexa Fluor 750, CD45-Krome Orange, and HLA-DR-SuperNova 780 (all from Beckman Coulter). After 20 min incubation at room temperature, samples were directly resuspended in a final volume of 300 μL of filtered water for acquisition. Filtered water was used to exclude the presence of background and noise signals, while an unstained sample was employed as negative control. Samples were acquired on a DxFlex cytometer (Beckman Coulter), equipped with violet (405 nm), blue (488 nm), and red (633 nm) lasers. Instrument daily quality control was carried out using CytoFlex Daily QC Fluorospheres (Beckman Coulter). Post-acquisition analysis was performed using FlowJo software (v.10.8.1; BD Biosciences). Particles were first identified based on simultaneous expression of Rhodamine and CD3, as correctly assembled BPLVs should have both PE-Rhodamine-conjugated lipids and CD3 derived from healthy lymphocyte membranes. On Rhodamine$^+$CD3$^+$ particles, expression of GPI-anchored proteins (Flaer$^+$), CD33, CD14, CD45, and HLA-DR was further investigated. Flow cytometry data were expressed as the percentage of positive BPLVs for a studied marker, or as median fluorescence intensity (MFI) for expression. MFI fold change (FC) was calculated for each studied marker as follows: MFI of stained sample / MFI of unstained sample.

BPLV cytotoxicity

PBMCs from healthy and PNH donors were seeded in a 96-well plate at a seeding density of 1x10^6 cells/mL, cultured in RPMI supplemented 10% FBS decomplemented (Gibco) and 1% Penicillin/Streptomycin solution (Corning Cellgro, Manassas, VA, USA). Empty and loaded BPLVs were added to culture media at a concentration of 0.1, 0.2, 0.5, 1 and 2 mg/mL (respect to lipid concentration after BPLV production) for 24h. 0.5 mg/mL of BPLVs were added to culture media for 24, 48 and 72h. After incubation at 37°C temperature and 5% CO_2, cell metabolic activity was analyzed using the 3-(4,5-Dimethylthiazol-2-yl)-2,5-diphenyl- tetrazolium bromide (MTT) assay. MTT at 0.5 mg/mL was added and incubated for 4h. Then, 96-well plates were centrifuged at 300g for 10 min, culture media was completely aspirated, and formazan products were dissolved in 200 μl of DMSO in each well. Absorbance was measured at 490 nm, after 5 min of gentle agitation at room temperature using a microplate reader (Infinite F200 PRO, Tecan Group Ltd., SW). All assays were performed in biological and technical triplicate (N = 3). Cells metabolic activity was calculated as a percentage with respect to the control group (considered as 100%), according to Equation 1.

$$\text{Cells metabolic activity (\%)} = \frac{Abs\ of\ sample - Abs\ of\ blank}{Abs\ of\ control - Abs\ of\ blank} \times 100 \quad \text{(Equation 1)}$$

Red blood cell uptake analysis

For red blood cell (RBC) uptake study, 100 μL of whole heparinized PB were diluted in 10 mL of PBS and centrifuged at 2200 rpm for 10 min. Next, pellets were resuspended in 10 mL of PBS, and 1mL of sample was stained with 5μL of Vybrant DiO cell labeling solution for staining membrane lipids (Thermo Fisher Scientific), incubated at 37°C on a shaker for 20 min, washed with 2mL of phosphate buffer saline (PBS; Gibco), and centrifuged at 2200 rpm for 10 min. Subsequently, DiO-labeled RBCs were seeded in a 6-well plate with RPMI supplemented with 10% of decomplemented FBS and 1% Penicillin/Streptomycin, and were treated or not with PE-Rhodamine-conjugated BPLVs at a final concentration of 0.5 mg/mL at 37°C and 5% CO_2 for 2h. After incubation, cells were harvested, washed with PBS, centrifuged at 2200 rpm for 10 min, and then resuspended in 1mL of PBS for centrifugation in a cytospin at 1500 rpm for 6 min. Subsequently, cells were washed with PBS and counterstained using 4′,6-diamidino-2-phenylindole (DAPI) to exclude the presence of nucleated cells. Images were acquired at 63x magnification with identical settings of light, exposure time, and gain using Leica laser-scanning confocal microscope (mod. TCS SP5; Leica Microsystems, Wetzlar DE).

PBMC uptake analysis

To investigate the ability of PBMCs to uptake BPLVs, a total of $1x10^6$ cells were seeded in a 12-well plate in RPMI supplemented with 10% of decomplemented FBS and 1% of Penicillin/Streptomycin with or without BPLVs at a final concentration of 0.5 mg/mL. Cells were then incubated at 37°C and 5% CO_2 for 24h, 48h, and 72h, while a sample immediately after seeding was kept as baseline control (T0). At each time point, cells were harvested, washed with PBS, centrifuged at 500g for 10 min, and cell pellets fixed in 4% PFA for 20 min at room temperature. After centrifugation at 500g for 10 min, cell pellets were resuspended in 200μL of PBS and kept at 4°C until use.

To investigate cellular mechanisms of BPLV uptake, a total of $5x10^4$ cells from healthy and PNH subjects were seeded in a 24-well plate in RPMI supplemented with 10% of decomplemented FBS and 1% of Penicillin/Streptomycin without any treatment, with only a reversible clathrin/dynamin inhibitor Dyngo-4a (Abcam, Milan, Italy) at 30 μM,[45] or with Dyngo-4a at 30 μM and BPLVs at 0.5 mg/mL for 2h, 5h, and 12h. Cells were pre-treated with Dyngo-4a for 15 min,[45] and then vesicles were added where appropriate. At each time point, cells were harvested, washed with PBS, centrifuged at 500g for 10 min, and cell pellets fixed in 4% PFA for 20 min at room temperature. After centrifugation at 500g for 10 min, cell pellets were resuspended in 500μL of PBS and kept at 4°C until analysis by confocal microscopy as described below.

Flow cytometry

After incubation with or without BPLVs, immunophenotyping was performed by staining a minimum of $1x10^6$ cells with the following antibodies according to the manufacturers' instructions: FLAER-AlexaFluor 488, CD3-ECD, CD33-PC5.5, CD14-Alexa Fluor 750, CD45-Krome Orange, and HLA-DR-SuperNova 780 (all from Beckman Coulter). After 20 min incubation at room temperature, cells were washed with phosphate-buffered saline (PBS) (IsoFlow Sheath Fluid, Beckman Coulter), and then resuspended in 500 μL of PBS for acquisition. Samples were acquired on a DxFlex cytometer (Beckman Coulter), equipped with violet (405 nm), blue (488 nm), and red (633 nm) lasers. Instrument daily quality control was carried out using CytoFlex Daily QC Fluorospheres (Beckman Coulter). Samples were run using the same PMT voltages, and at least 200,000 events were recorded. Post-acquisition analysis was carried out using Kaluza Analysis Flow Cytometry Software v2.1.1 (Beckman Coulter). First, cells were identified based on linear parameters (forward side scatter-area [FSC-A] vs side scatter-area [SSC-A]), and double cells removed (FSC-A vs FSC-height [FSC-H]). On single cells, $Rhodamine^+Flaer^+$, $Rhodamine^+CD3^+$, $Rhodamine^+CD33^+$, $Rhodamine^+CD14^+$, and $Rhodamine^+HLA\text{-}DR^+$ cells were gated. Flow cytometry data were expressed as the percentage of positive cells or as MFI for expression of each studied marker. Radar plots were also employed for simultaneous visualization of all studied markers.

Confocal imaging

After incubation with or without BPLVs, 2×10^5 of PBMCs were fixed with 2% PFA before staining protocol. Then, cells were stained for anti-FLAER antibody FITC conjugated (Beckman Coulter) for 20 min at RT in the dark. Subsequently, cells were washed with PBS 1X and counterstained using 4',6-diamidino-2-phenylindole (DAPI). All images were acquired at 63x magnification with identical settings of light, exposure time, and gain using Leica laser-scanning confocal microscope (mod. TCS SP5; Leica Microsystems, Wetzlar DE).

Lysis test

To test resistance to complement-mediated lysis after BPLV treatment, a total of $1x10^6$ PBMCs from healthy subjects and PNH patients were first incubated without or with BPLVs at a final concentration of 0.5 mg/mL for 48h in a 12-well plate using RPMI supplemented with 10% of decomplemented FBS and 1% Penicillin/Streptomycin at 37°C and 5% CO_2. Subsequently, cells were washed, and culture medium was replaced with fresh medium containing RPMI plus 1% Penicillin/Streptomycin and 10% decomplemented or normal FBS. Samples were incubated for 2h or 24h at 37°C and 5% CO_2, and then washed with 1mL of PBS. After centrifugation, cells were stained with 3 μL of Fixable Viability Dye eFluor™ 780 (eBioscience™) after reconstitution and dilution as per manufacturers' instruction, incubated for 15 min at room temperature, washed with 2mL of PBS, centrifuged at 500g for 10 min, and then resuspended in 100 μL of 2% PFA for acquisition. Samples were acquired on a DxFlex cytometer (Beckman Coulter), and post-acquisition analysis was carried out using Kaluza Analysis Flow Cytometry Software v2.1.1 (Beckman Coulter). Total cells were first gated for PE-Rhodamine BPLV and Viability dye parameters, and $BPLV^+$ live and $BPLV^+$ dead cells, or $BPLV^-$ live and $BPLV^-$ dead cells were identified. Based on the hypothesis that $BPLV^+$ should have uptake also endogenous complement inhibitors, such as CD55 and CD59, or other GPI-linked proteins, $BPLV^+$ cells should be more resistant to complement-mediated lysis induced by addiction of normal FBS to culture medium. Therefore, we calculated a ratio between dead and live cells in $BPLV^+$ and $BPLV^-$ populations, as cells more susceptible to lysis should display a higher ratio (dead cells >> live cells), while cells more resistant to complement-mediated lysis a lower ratio (live cells >> dead cells).

Cell viability was also assessed by MTT assay. PBMCs from healthy and PNH subjects were seeded in a 96-well plate at a seeding density of $1x10^6$ cells/mL, cultured in RPMI supplemented 1% Penicillin/Streptomycin solution (Corning Cellgro, Manassas, VA, USA), plus 10% of normal FBS (Gibco) with and without loaded BPLVs at a concentration of 0.5 mg/mL (respect to lipid concentration after BPLV production) for 24h. PBMCs from healthy and PNH donors cultured in RPMI supplemented 1% Penicillin/Streptomycin solution plus 10% of decomplemented FBS were used as controls. After incubation at 37°C and 5% CO_2, cell metabolic activity was analyzed using the 3-(4,5-Dimethylthiazol-2-yl)-2,5-diphenyl-tetrazolium bromide (MTT) at 0.5 mg/mL. MTT was incubated for 4h; then, 96-well plates were centrifuged at 300g for 10 min, culture media was completely aspirated, and formazan products were dissolved in 200μl of DMSO in each well. Absorbance was measured at 490 nm, after 5 min of gentle agitation at room temperature using a microplate reader (Infinite F200 PRO, Tecan Group Ltd., SW). All assays were

performed in biological and technical triplicate (N = 3). Cells metabolic activity was calculated as a percentage with respect to the control group (considered as 100%), according to Equation 1 as shown above.

QUANTIFICATION AND STATISTICAL ANALYSIS

Data were collected from a computerized database and chart review and were analyzed using Prism (v.9.4.1; GraphPad software, La Jolla, CA, US). The number of replicates for each analysis was three (biological and technical triplicate). Paired or unpaired two-tailed t-test was employed for two group comparisons, while multiple comparisons for percentage of positive cells, MFI values, or live/dead ratios between each sample and timepoint were performed using one-way analysis of variance (ANOVA) fitting a main effects only model and uncorrected Fisher's LSD. Data are represented as mean $\pm$ SD. A P value < 0.05 was considered statistically significant.